The Astrophysical Journal Letters, 896:L43 (10pp), 2020 June 20 https://doi.org/10.3847/2041-8213/ab9900

The Accuracy of the Hubble Constant Measurement Verified through Cepheid Amplitudes

Adam G. Riess[1,2], Wenlong Yuan[2], Stefano Casertano[1,2], Lucas M. Macri[3], and Dan Scolnic[4]
[1] Space Telescope Science Institute, 3700 San Martin Drive, Baltimore, MD 21218, USA
[2] Department of Physics and Astronomy, Johns Hopkins University, Baltimore, MD 21218, USA
[3] Texas A&M University, Department of Physics and Astronomy, College Station, TX 77845, USA
[4] Duke University, Department of Physics, Durham, NC 27708, USA
Received 2020 May 1; revised 2020 May 29; accepted 2020 May 31; published 2020 June 22

Abstract

The accuracy of the Hubble constant measured with extragalactic Cepheids depends on robust photometry and background estimation in the presence of stellar crowding. The conventional approach accounts for crowding by sampling backgrounds near Cepheids and assuming that they match those at their positions. We show a direct consequence of crowding by unresolved sources at Cepheid sites is a reduction in the fractional amplitudes of their light curves. We use a simple analytical expression to infer crowding directly from the light curve amplitudes of >200 Cepheids in three Type Ia supernovae hosts and NGC 4258 as observed by Hubble Space Telescope—the first near-infrared amplitudes measured beyond the Magellanic Clouds. Where local crowding is minimal, we find near-infrared amplitudes match Milky Way Cepheids at the same periods. At greater stellar densities we find that the empirically measured amplitudes match the values predicted (with no free parameters) from crowding assessed in the conventional way from local regions, confirming their accuracy for estimating the background at the Cepheid locations. Extragalactic Cepheid amplitudes would need to be ∼20% smaller than measured to indicate additional, unrecognized crowding as a primary source of the present discrepancy in H_0. Rather, we find the amplitude data constrains a systematic mis-estimate of Cepheid backgrounds to be 0.029 ± 0.037 mag, more than $5\times$ smaller than the size of the present ∼0.2 mag tension in H_0. We conclude that systematic errors in Cepheid backgrounds do not provide a plausible resolution to the Hubble tension.

Unified Astronomy Thesaurus concepts: Cepheid distance (217); Hubble constant (758); Cosmology (343); Distance indicators (394); CCD photometry (208); Light curves (918); Cepheid variable stars (218)

Supporting material: machine-readable tables

1. Introduction

A leading approach to measure the Hubble constant (H_0) locally uses Hubble Space Telescope (HST) observations of Cepheid variables in the hosts of recent, nearby Type Ia supernovae (SNe Ia) to build a three-rung distance ladder (Riess et al. 2016, hereafter R16). Cepheids are favored as primary distance indicators because they are very luminous ($M_V \approx -6$ mag), extremely precise (3% in distance per source, Riess et al. 2019, hereafter R19), easy to identify due to their periodicity (Leavitt & Pickering 1912), and well understood as a consequence of stellar pulsation theory (Eddington 1917). They are also the best calibrated tool for this role when a consistent photometric system is used along the distance ladder. HST Wide Field Camera 3 (WFC3)/ultraviolet and visible light (UVIS) and infrared (IR) have been used by the SH0ES Team (R19) to measure Cepheids in supernova (SN) hosts and for three independent sources of geometric distance calibration of their luminosities: the megamaser host NGC 4258, the Milky Way (MW; and its parallaxes), and the Large Magellanic Cloud (LMC; via detached eclipsing binaries). Near-infrared (NIR) observations are particularly valuable and are employed to overcome the twin pitfalls of metallicity and dust, which limited the first-generation measurements made in the optical (Freedman et al. 2001; Sandage et al. 2006).

However, all long-range distance indicators have shortcomings. For measurements of Cepheids at $D \geqslant 10$ Mpc, even with their great luminosity and the resolution of HST, it is often not possible to separate Cepheids from their stellar crowds. Unlike SNe, which fade away to offer a clear view of what lies in their midst, Cepheids modulate their brightness but do not vanish. It is therefore necessary to *statistically* estimate the background flux using nearby regions before we can assess the true flux of a Cepheid. Hereafter, we will refer to the superposition of stellar flux on a Cepheid as "crowding." The fact that these backgrounds are not smooth, but rather composed of unresolved point sources, adds noise to a statistical estimate of the background and hence that of the Cepheid flux. As Freedman et al. (2019, p. 13) noted, "possibly the most significant challenge for Cepheid measurements beyond 20 Mpc is crowding and blending from redder (RGB and AGB) disk stars, particularly for NIR *H*-band measurements of Cepheids."

This challenge is not unique to Cepheid photometry. Since the advent of charge-coupled devices (CCDs) and the desire to measure stellar photometry in dense fields, software tools to measure "crowded-field photometry" have used knowledge of the point-spread function (PSF) to simultaneously constrain the positions and fluxes of overlapping stars and a more uniform background level of unresolved fluctuations (Stetson 1987; Mateo & Schechter 1989). A drawback of such measurements is that they necessarily rely on the assumption that the background flux *near Cepheids* has the same mean as that at the positions of Cepheids. This would seem a fair assumption because our line of sight to a Cepheid, which determines which stars will be superimposed on the Cepheid, is inherently random. However, the assumption could fail in the presence of stars *physically associated* with the Cepheid and could become

important for the distance ladder if the associated flux is not resolved at the distance of SN Ia hosts, but is resolved at the distance Cepheids are geometrically calibrated, a physical scale of 400 astronomical units to a few parsecs for Cepheids measured at $D \geqslant 10$ Mpc and calibrated with MW parallaxes. A wide-binary or host cluster could be the source of such flux. Mochejska et al. (2000) claimed a strong bias from this source in optical Cepheid photometry from the HST Key Project (KP) and the low-resolution Wide Field and Planetary Camera 2 (WFPC2) based on binning ground-based images of M31. However, Ferrarese et al. (2000) demonstrated that the effect was quite negligible in the KP data after simulating *the selection* of extragalactic Cepheids using artificial star tests. These tests account for how the underlying sky is brightened and include the impact on the measured PSF and Cepheid light curve, both metrics for selecting Cepheids. Ferrarese et al. (2000) further cited a factor that they stated was "not easily quantifiable"—such contamination would decrease the amplitude of the Cepheid light curve, reducing its likelihood of being selected. Anderson & Riess (2018; see also Senchyna et al. 2015) used HST imaging of M31 to resolve the clusters near Cepheids in the bands used by SH0ES (R19). They found that the associated flux from clusters can be substantial, with a mean of 0.3 mag, but the fraction of Cepheids in such clusters (and close enough to their centers to be unresolved at the distances of SN Ia hosts) is very low, ∼2.5%, so the resulting bias on H_0 from the product of the two is <0.01 mag. The low fraction of Cepheids seen in clusters is because the cluster dispersement timescale is a factor of ∼5 shorter on average than Cepheid ages (Anderson & Riess 2018). This is reassuring for the goal of reaching a 1% determination of H_0, but does depend on the plausible assumption that the fraction of Cepheids in clusters in M31 is similar to those of the large spirals of SN Ia hosts used to build the distance ladder.

In light of the present discrepancy between the locally measured value of H_0 and the value inferred from the early universe in concert with the cosmological model (see Riess 2019, for a review) and the possibility that it raises of new physics, it is necessary to subject all aspects of these measurements to increasingly higher levels of scrutiny. Therefore, it is important to identify a *direct* measure of the crowding of Cepheids in SN Ia hosts used for the determination of H_0 which is also independent of resolution and hence distance.

Here we present a new method that *directly* tests the accuracy of crowded-field Cepheid photometry and the key assumption that superimposed flux due to crowding can be accurately estimated from its annular vicinity. Crowding decreases the amplitude of a Cepheid measured *in magnitudes*, due to its greater fractional contribution at minimum versus maximum light. Thus the observed amplitude of a Cepheid provides a direct test of this assumption. In Section 2 we describe crowding and derive a simple mathematical function that relates the apparent amplitude of a Cepheid to its crowding with no free parameters. In Section 3 we calibrate the amplitudes of MW Cepheids as a function of their period to use as a benchmark to compare to extragalactic Cepheids in the absence of crowding, and in Section 4 we present the first sample of distant NIR extragalactic Cepheid light curve amplitudes. By combining these amplitude–crowding and amplitude–period relations we show that the amplitudes of extragalactic Cepheids match the values expected if their locally measured crowding is the same as that at the position of the Cepheids, testing a crucial assumption of the distance ladder. This eliminates a possible systematic error at 5σ confidence for explaining the present discrepancy in H_0.

2. Amplitudes and Crowding

2.1. Crowding

The SH0ES program identifies Cepheids and measures their periods using 11–15 epochs of optical HST imaging in the hosts of recent SNe Ia and follows these identifications with NIR Cepheid photometry (Riess et al. 2009). Time-sampled imaging centered near the visual band (∼0.5 μm) coupled with the fine $0\farcs04$ pixel^{-1} sampling of WFC3-UVIS and PSF-fitting provides Cepheid photometry at $D = 20$–40 Mpc with minimal crowding measured to be ∼2% of the Cepheid flux (Hoffmann et al. 2016). However, in the NIR the resolution and pixel sampling is a factor of ∼3 lower (i.e., for WFC3-IR in the F160W, the band is centered at ∼1.5 μm and has $0\farcs13$ pixel^{-1}), and thus the background area and number of potential stellar contaminators is an order of magnitude greater than in the optical. In addition, the dominant sources of Cepheid crowding in the NIR are red giants, and thus the contrast with the bluer Cepheids is less relative to optical passbands (for examples, see Figure 8 in Riess et al. 2009). As a result, the flux from crowding that is within the resolution element of NIR imaging with HST can rival the flux of the Cepheid.[5]

To accurately measure Cepheid photometry it is therefore critical to characterize and account for the mean level of crowding, which is most readily achieved by adding and measuring artificial stars of the same brightness as each Cepheid, placed randomly in its vicinity. It is advantageous and most compact to quantify the crowding offset and its dispersion in the units of the difference between the input and output magnitude of the artificial stars, because these values have been empirically shown to be distributed as log-normal in flux or Gaussian in magnitudes out to a few standard deviations due to the distribution of background sources whose numbers decrease with increasing flux (Riess et al. 2009).

In magnitude space, we define the crowding, Δm, as the difference between the true magnitude m_0, corresponding to flux F_0, and the apparent measured magnitude m', corresponding to the blended flux $F_0 + F_1$.

A crucial advantage for NIR follow-up of optical discoveries is that the Cepheid position in the NIR scene is fixed by the optical image, which constrains the fit and lowers the uncertainty in the NIR measurement. A further refinement of the analysis for each Cepheid comes from measuring the displacement of its detected position in the NIR image from its optically determined position, a measure of the *specific* degree of blending. The artificial star trials used to characterize the crowding are selected from those with similar displacements (Riess et al. 2009). Lastly, the estimate of the input magnitude

[5] Photometry measured by summing the flux in apertures after sky subtraction naturally removes the statistical contribution of crowding because it is included in the mean sky level per-pixel, but this method is otherwise disadvantageous in dense regions because it cannot separate overlapping sources using knowledge of the PSF nor does it use the PSF as weights for the target's pixels, which improves signal-to-noise. The need to explicitly account for crowding in PSF photometry results from full blending of background sources with the target PSF rendering the multi-source model degenerate to the presence of such blended sources. Therefore, the presence of such blended sources is inferred statistically from the local stellar density and measured using artificial stars.

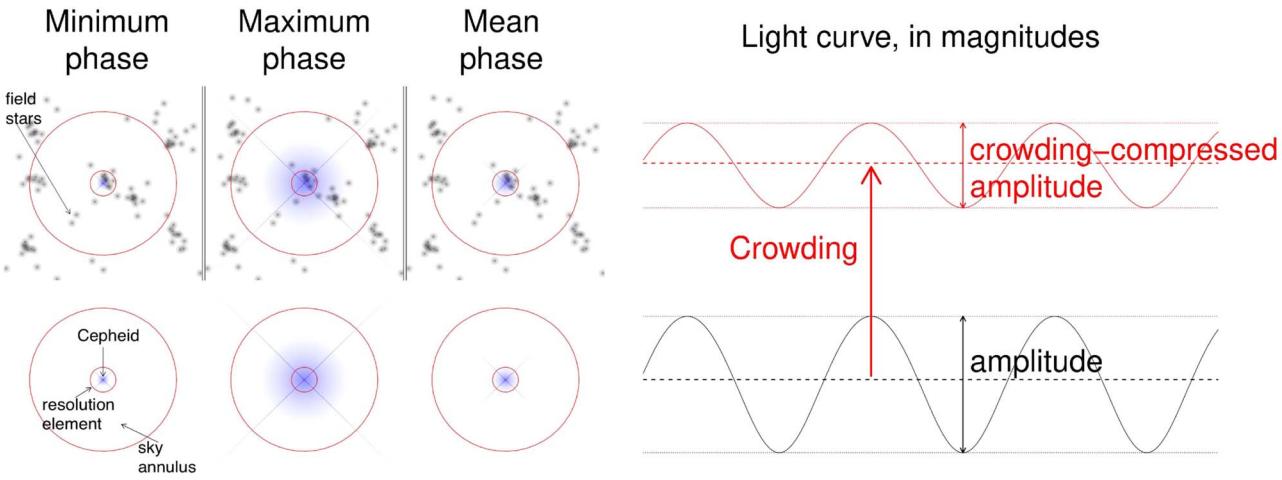

Figure 1. Illustration of the relation between crowding and apparent amplitude in magnitude space. Top left: crowded case, photometry of a Cepheid includes flux from field stars contained in its resolution element. The resulting light curve in magnitude space (upper right) is brighter (i.e., crowding) and its amplitude is compressed (because magnitudes measure fractional flux and the fractional contribution of the field stars flux is greater at minimum phase than at maximum phase) Bottom panels: uncrowded case.

for the artificial stars is derived independent of the measured magnitude of the Cepheid by using an estimate derived from its period and the crowding-corrected period-magnitude relation of its host brethren. This is necessarily an iterative approach as each loop produces a more accurate determination of the unbiased period–luminosity relation.

2.2. Amplitudes

In Figure 1 we illustrate how crowding alters the measurement of the amplitude of a Cepheid. We can derive a simple relation for the measured amplitude of a symmetric light curve in magnitude space in the presence of background light. The approximation is valid for a generic light curve shape, but for definiteness we consider a sinusoidal curve—which is a good approximation to a Cepheid light curve in the F160W band. For a variable flux source

$$F(t) = F_0 * (1 + \delta(t)) \quad (1)$$

where the mean flux $\langle F \rangle = F_0$ and we assume for simplicity $\delta = \alpha * \sin(2\pi t/P)$, where P is the period of the variable. Let us define α as the maximum value of $\delta(t)$; because of symmetry, the minimum value is $-\alpha$. The fractional flux amplitude a is then

$$a \equiv (\max(F) - \min(F))/\langle F \rangle = \delta_{\max} - \delta_{\min} = 2\alpha. \quad (2)$$

Now assume that the same source is blended with another source of constant flux F_1. The apparent light curve will then be

$$F' = F_0 * (1 + \delta(t)) + F_1 \quad (3)$$

and the apparent fractional flux amplitude a' will be

$$a' = (\max(F') - \min(F'))/\langle F' \rangle = a * (F_0/(F_0 + F_1)) \quad (4)$$

so that the flux amplitude will be compressed by a factor $F_0/(F_0 + F_1)$. From the definition of Δm,

$$F_0/(F_0 + F_1) = 10^{-0.4*m_0}/10^{-0.4*m'} = 10^{-0.4*\Delta m} \quad (5)$$

while from the definition of the amplitude in magnitude space, A (the difference between the minimum and maximum magnitude) is

$$A = 2.5\log_{10}[(1 + \alpha)/(1 - \alpha)] \sim 1.0857a + O(\alpha^3) \quad (6)$$

where we have used the linear approximation for $\log[(1 + x)/(1 - x)] \approx 2 * x + O(x^3)$, and the factor $1.0857 \approx 2.5/\log(10)$ converts from magnitudes to natural logarithms.

When the source is blended, the amplitude in magnitude, A', will similarly follow:

$$A' \approx 1.0857a' + O(\alpha^3). \quad (7)$$

From Equations (4) and (5), we obtain to second order in the amplitude the ratio of the apparent to the true amplitude in magnitude space:

$$A'/A = 10^{-0.4*\Delta m}. \quad (8)$$

The approximation is better than 0.0005 mag in A' for $0 < \Delta m < 2$ as we show for two example light curves, a sinusoid and a sawtooth-like, in Figure 2.

As Equation (8) shows, in the low-crowding case $\Delta m \sim 0$, the observed amplitude A' is the same as the true, A, as expected. For very large crowding $\Delta m \gg 1$, $A' \sim 0$, also as expected. Equation (8) shows that the apparent amplitude of a Cepheid, A', provides a direct measure of its crowding as long as the true amplitude A can be estimated a priori. Thus, measuring the apparent amplitude offers the means to test the accuracy of the crowding measured from nearby regions. To make use of this relation we first need to determine the true amplitudes of Cepheid variables.

3. Calibrating the Cepheid Amplitude–Period Relation in the MW

We use MW Cepheids to calibrate the relation between Cepheid amplitudes and periods in the absence of crowding—including the statistical contribution of close unresolved binaries. These will provide the values of A in Equation (8) to compare to the observed amplitudes.

It is well known that the amplitudes of Cepheids vary in a somewhat predictable way with period following the "Hertzsprung Progression" (Hertzsprung 1926), though they exhibit a

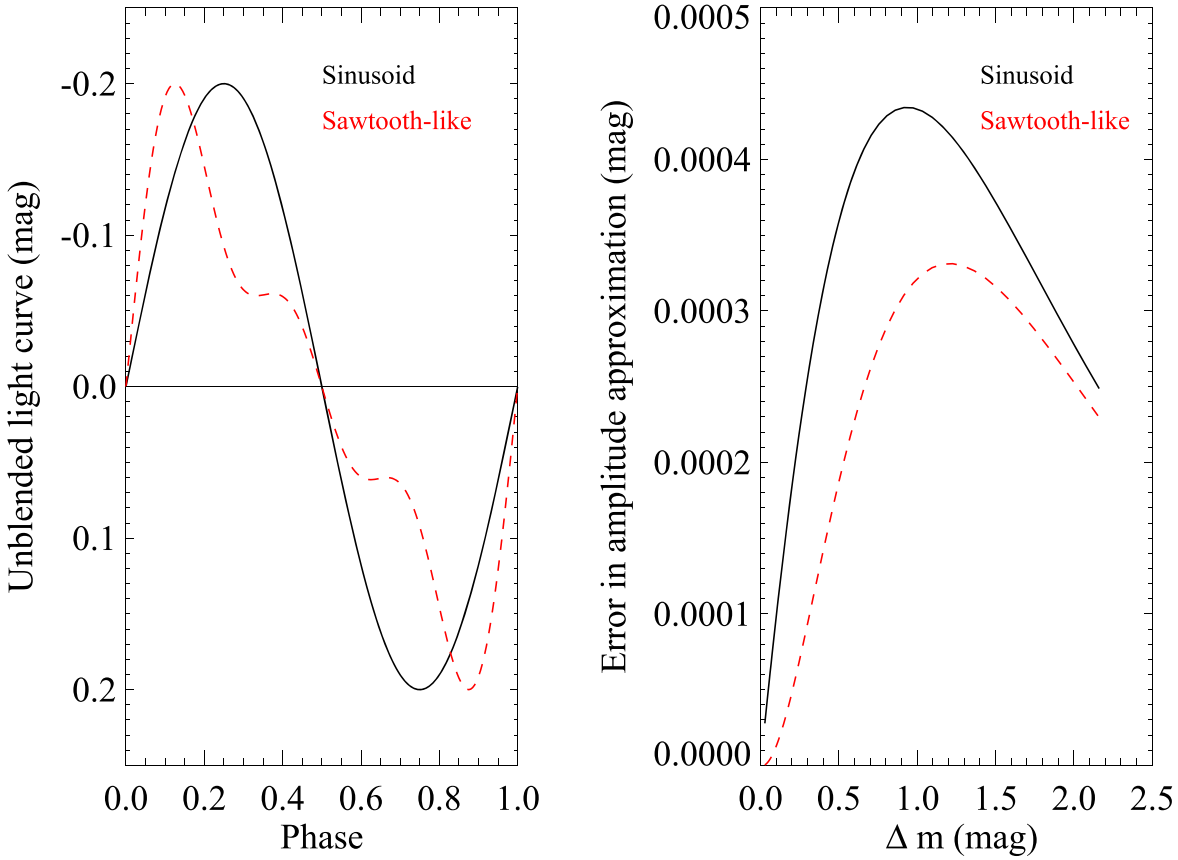

Figure 2. Numerical vs. analytical approximation for computing the impact of crowding on amplitude. Two example light curves are given on the left: a sinusoid and a sawtooth. The difference between a numerical computation vs. the analytical approximation of Equation (8) is shown on the right. As shown, the analytical approximation is good to 0.2%, a far smaller difference than other sources of uncertainty.

sizable range at a given period. In Figure 3 and Table 1 we show the amplitudes of 56 MW Cepheids with $P > 10$ days as a function of their periods. This is the range of periods relevant for the detection of the extragalactic Cepheids. This sample contains most of all known in the MW and all with readily available V- and H-band light curves, which could be used to determine accurate values of their visual and H-band amplitudes, A^V and A^H, respectively. The sources of light curves are Laney & Stobie (1992), Monson & Pierce (2011), and Riess et al. (2018).

The H-band amplitude, A^H, has a mean value of ∼0.4 mag in this period range but with a rather large dispersion of ∼0.1 mag. The visual band amplitude, A^V, has a mean value of ∼1.0 mag and a dispersion of ∼0.2 mag. However, their ratio, $\frac{A^H}{A^V}$, has a factor of three times lower variation at a given period than A^H. This may be expected because the same physical pulsation produces both amplitudes so the ratio has little variation. In Figure 3 we see a fairly simple trend of the amplitude ratio A^H/A^V with period, which can be fit to good accuracy by a quadratic. A linear trend for the amplitude ratio with period does nearly as well, although it does not capture a slight flattening of the ratio at long periods.

Thus we can predict the H-band amplitude for an extragalactic Cepheid on the basis of its period, and if available, its visual amplitude with good precision. We recast Equation (8) to relate the V-to-H amplitude ratio in the presence of crowding (i.e., the primed amplitudes) to the uncrowded (i.e., MW and unprimed) values as

$$\left(\frac{A'^H}{A'^V}\right)\Big/\left(\frac{A^{H,\mathrm{MW}}}{A^{V,\mathrm{MW}}}\right) = 10^{-0.4*(\Delta m_H - \Delta m_V)} \quad (9)$$

Finally, to compare MW Cepheids in V- and H-bandpasses to extragalactic Cepheids (which are measured in similar bandpasses with overlapping wavelengths: F350LP, F555W, and F160W) we derived and applied the following transformations to the MW amplitudes:

$$A^{\mathrm{F350LP}} = A^V/(0.984 + 0.296 * (\log P - 1.5)) \quad (10)$$

and

$$A^{\mathrm{F160W}} = 1.015 * A^H. \quad (11)$$

We derived the transformation between F350LP and V from observations of the same Cepheids in both F350LP and F555W in NGC 5584 (Hoffmann et al. 2016). We derived transformations between ground and HST equivalent bandpasses using a subset of Cepheids with multicolor data V, I, J, H resulting in Equation (11) and $A^V = 1.04 * A^{\mathrm{F555W}}$.

As the transformations show, the amplitudes differ by only a few percent so these corrections have minimal impact on the final results but are included for accuracy. It may be worth noting that the transformations are needed because the empirically measured amplitudes (in the MW) are in a different photometric system than the amplitudes measured in SN Ia host galaxies. If we did not correct for band-dependent ratios, we could under- or overestimate the predicted unblended

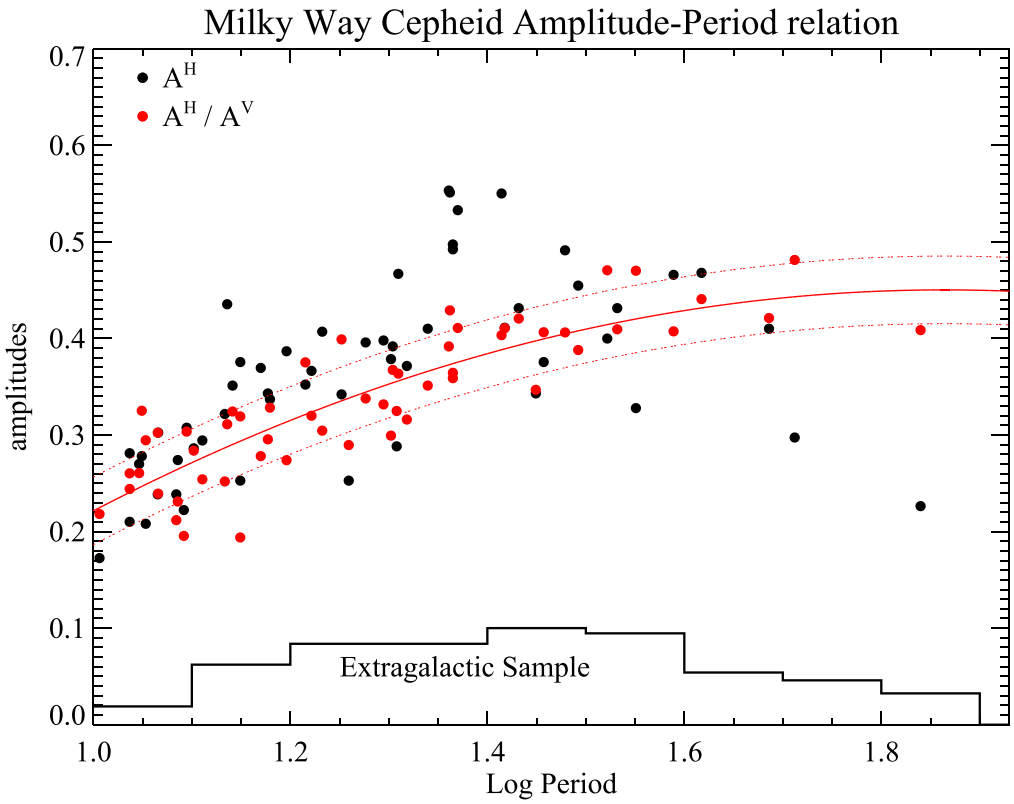

Figure 3. Relation between light curve amplitude and period from MW Cepheids with log$P > 1$. H-band amplitudes (A^H) are plotted using black circles, while red symbols denote the amplitude ratio A^H/A^V. The red line shows a quadratic fit to this data and is used to model this amplitude ratio as a function of period. The histogram at the bottom shows the period distribution of extragalactic Cepheids whose amplitudes will be compared to MW Cepheids.

amplitudes, leading to an imprecise result. For simplicity, hereafter we will refer to the amplitudes whether originally measured in F350LP, F555W, or V but now transformed to the F350LP system via these relations as A^V (primed and unprimed), and for amplitudes measured in F160W or H but now on the F160W system via Equation (11) as A^H (primed and unprimed).

Thus we characterize the amplitude ratio for MW Cepheids of a given period (and as shown in Figure 3) as

$$\frac{A^{H,\mathrm{MW}}}{A^{V,\mathrm{MW}}} = 0.22 + 0.53(\log P - 1) - 0.31(\log P - 1)^2 \quad (12)$$

with a dispersion of 0.035. We now proceed to use this relation to compare to the measured amplitude ratios of extragalactic Cepheids of known periods in the presence of a range of crowding.

4. NIR Amplitudes of Extragalactic Cepheids versus Local Crowding

4.1. Extragalactic Amplitude Measurements

We used multi-epoch NIR imaging with WFC3, listed in Table 2 and designed to find Mira variables, to measure light curves and amplitudes of optically identified Cepheids. Such observations are available for SN Ia hosts NGC 5643, NGC 1559, and NGC 2525 and for NGC 4258, the megamaser host used for the geometric calibration of Cepheid luminosities.

We obtained multi-epoch NIR Cepheid photometry using the DAOphot and ALLSTAR packages (Stetson 1987; Stetson et al. 1990). Example light curves and their host regions are shown for Cepheids identified optically in F350LP in NGC 1559, the most distant host in our sample at $D \sim 20$ Mpc, in Figure 4. These display a range of apparent amplitudes and local stellar densities.

To help measure the NIR amplitudes we use optical light curves, which have greater leverage to constrain the period and phase of each Cepheid. Thus we limit the number of parameters used to fit the NIR light curves to two: the mean magnitude and amplitude of a sinusoidal function. We include a mean phase offset between the NIR and visual light curves of 0.3 (as derived by Soszyński et al. 2005, from the mean of many MW light curves) and propagate an amplitude uncertainty of $\sigma = 0.04$ mag, which translates into a 10% uncertainty in A'^H. Example light curve fits are shown in Figure 4. The exception was for the host NGC 4258 where the NIR and optical data were obtained far apart in time so we added a third, phase-shift parameter between the NIR and optical data for these fits.

In Table 3 we give the measured visual and NIR amplitudes of 224 Cepheids across four hosts that provided good-quality light curve fits, their locally derived crowding corrections in the V- and H-bands, and periods. The crowding corrections, Δm_H, were determined from artificial star injection and retrieval following the same procedure and software used by R16 and described in Section 2.

Artificial star tests demonstrate that Cepheid measurements in visual bands (F555W or F350LP) at these distances with WFC3 suffer from very little crowding (Hoffmann et al. 2016), and we find mean values of Δm_V of 0.009, 0.027, 0.020, and 0.020 mag for NGC 5643, NGC 1559, NGC 2525, and NGC 4258, respectively. The first three were obtained with F350LP and NGC 4258 with F555W imaging. From Equation (8) we thus expect the visual amplitudes to be reduced from their true

Table 1
Amplitude Data for MW Cepheids

Cepheid	Period	A^V	A^H
SY-Aur	10.15	0.663	0.170
VX-Per	10.89	0.684	0.207
Z-Lac	10.89	0.976	0.277
SV-Per	11.13	0.881	0.266
DR-Vel	11.20	0.728	0.274
AA-Gem	11.30	0.602	0.205
RX-Aur	11.62	0.675	0.235
UU-Mus	11.64	1.082	0.298
RY-Cas	12.14	0.970	0.235
KK-Cen	12.18	1.022	0.270
SS-CMa	12.35	0.982	0.219
XY-Car	12.44	0.876	0.303
SY-Nor	12.65	0.874	0.282
Z-Sct	12.90	1.007	0.290
AD-Pup	13.60	1.119	0.317
BN-Pup	13.67	1.227	0.429
CY-Aur	13.85	0.951	0.346
SV-Vul	14.10	1.036	0.370
SV-Vel	14.10	1.148	0.249
RW-Cas	14.79	1.178	0.364
VW-Cen	15.04	1.032	0.338
SZ-Cyg	15.11	0.913	0.332
XX-Car	15.71	1.263	0.381
RW-Cam	16.42	0.845	0.347
XZ-Car	16.65	1.033	0.361
CD-Cyg	17.08	1.210	0.401
CP-Cep	17.86	0.781	0.337
YZ-Car	18.17	0.797	0.249
VY-Car	18.90	1.076	0.390
RU-SCT	19.70	1.108	0.392
KX-CYG	20.05	1.171	0.373
VX-CYG	20.14	0.988	0.386
RY-Sco	20.32	0.823	0.284
RZ-Vel	20.40	1.192	0.460
V340-Ara	20.81	1.094	0.366
WZ-Sgr	21.85	1.094	0.404
BM-PER	22.96	1.332	0.545
WZ-Car	23.01	1.212	0.543
VZ-Pup	23.17	1.309	0.490
VZ-Pup	23.17	1.276	0.485
SW-Vel	23.44	1.227	0.525
X-Pup	25.97	1.308	0.542
OT-PER	26.16	0.961	0.405
T-Mon	27.03	0.989	0.425
RY-Vel	28.13	0.959	0.338
KQ-Sco	28.66	0.898	0.370
AQ-Pup	30.12	1.183	0.484
V0609-CYG	31.06	1.151	0.448
V0396-CYG	33.25	0.842	0.394
KN-Cen	34.03	1.047	0.425
l-Car	35.55	0.697	0.323
U-Car	38.82	1.156	0.459
RS-Pup	41.44	1.082	0.461
V1467-CYG	48.53	1.012	0.404
GY-SGE	51.53	0.647	0.293
S-Vul	69.16	0.601	0.223

(This table is available in machine-readable form.)

values by only 1%–3%. As discussed in Section 2, due to increased pixel size, larger PSF FWHM, and reduced contrast, the F160W measurements have greater values of Δm_H. We have extended the Cepheid sample here to include objects found in high surface brightness regions and with much greater crowding than the limit typically used to measure H_0 such as in R16. The purpose of this extension is to increase the sensitivity of our sample for testing the relation between Cepheid amplitude and crowding. The median Δm_H for the "low-crowding" sample used to measure H_0 (R16) is 0.38 mag and for the "high-crowding" sample not typically used to measure H_0 but added here to increase our sensitivity to study crowding is 0.97 mag as indicated in Figure 5. In some cases for the high-crowding sample $\Delta m_H \sim 2.0$ mag, i.e., 5 times the Cepheid for the maximally crowded case.

Table 2
Multi-epoch Observations of Hosts in F160W

Host	Epochs	Exposure (s)	HST Programs	No. of Cepheids[a]
NGC 5643	9	1000	15145, 15640	102
NGC 1559	9	1000	15145	78
NGC 2525	13	900–1100	15145, 15693	15
NGC 4258i	12	2200	13445	27
NGC 4258o	4	1500	15640	2

Note.
[a] Cepheids with well-fit NIR light curves, $\sigma_{\rm amp} < 0.15$.

4.2. The Observed Crowding-amplitude Relation and Local Crowding

Following Equation (9), the crowding term, $\Delta m_H - \Delta m_V$, fully specifies the relation between the extragalactic (crowded) and MW (uncrowded) amplitude ratio with no free parameters so that

$$\left(\frac{A'^H}{A'^V}\right) = \left(\frac{A^{H,\rm MW}}{A^{V,\rm MW}}\right) 10^{-0.4*(\Delta m_H - \Delta m_V)} = (0.22 + 0.53(\log P - 1) - 0.31(\log P - 1)^2) \times 10^{-0.4*(\Delta m_H - \Delta m_V)}. \quad (13)$$

We substitute the polynomial expression relating $A^{H,\rm MW}/A^{V,\rm MW}$ to period in Equation (12), allowing us to predict the measured amplitude ratios of the extragalactic Cepheids solely from their periods and local crowding and thus without any free parameters on the right-hand side of Equation (13).

In Figure 5 we show the observed relation between the local crowding $\Delta m_H - \Delta m_V$ and the amplitude ratio of extragalactic to MW Cepheids (we note as discussed earlier, the term $(\Delta m_H - \Delta m_V) \sim \Delta m_H$ to good approximation).

Equation (13) predicts, and the measurements in Figure 5 show, that at $(\Delta m_H - \Delta m_V) \sim 0$ MW and extragalactic amplitude ratios are consistent. As crowding increases, the amplitude ratio for extragalactic Cepheids decreases and approaches zero. This is confirmed by comparing the fit of Equation (13) and a second-order polynomial fit constrained only by the data in Figure 5. We verify that this reduction in ratio with enhanced local crowding is due to the reduction in A^H (and not an increase in A^V) by examining the composite light curves of the F160W light curve points for Cepheids with high and low Δm_H in Figure 6.

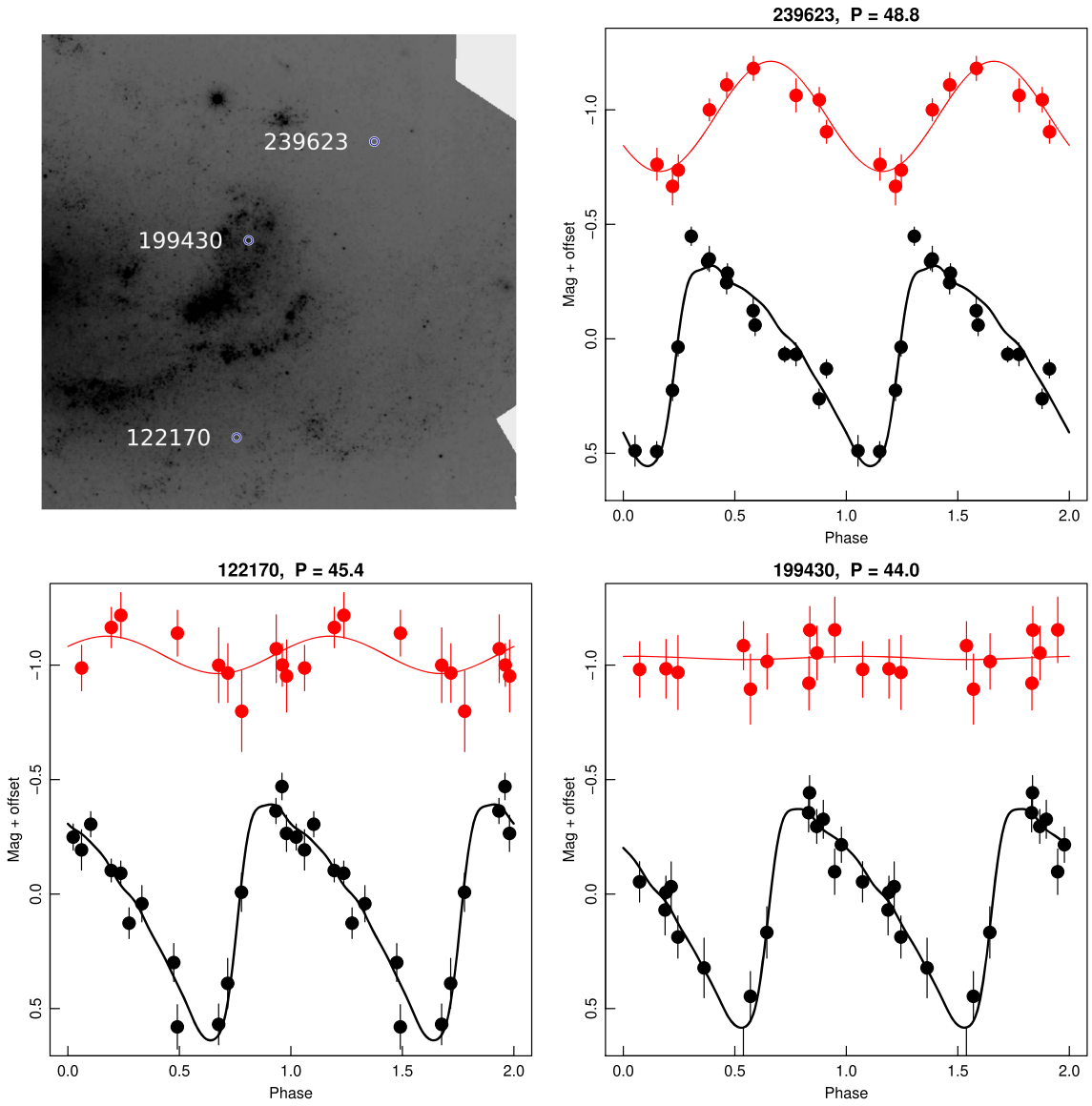

Figure 4. Three example light curves of Cepheids in NGC 1559, at $D = 20$ Mpc, the most distant in our sample. These showcase amplitudes that are nominal for MW Cepheids (top right), half as normal (bottom left) and minimal (bottom right), a progression that statistically follows their local stellar density as shown in the top left. The latter example is in a region with higher density than the limit imposed for measurements of H_0. Black points are from F350LP and red from F160W.

Next we define a standard χ^2 statistic to assess the goodness of fit of Equation (13):

$$\chi^2 = \sum_{i=1}^{n} \left(\frac{A'^H}{A'^V} - \frac{A^{H,\mathrm{MW}}}{A^{V,\mathrm{MW}}} 10^{-0.4*(\Delta m_H - \Delta m_V)} \right)^2 \sigma_i^{-2}. \quad (14)$$

The model error in the amplitude ratio, σ_i, is the quadrature sum of the amplitude measurement error propagated from the DAOphot photometry errors, the dispersion of the local crowding estimate times the amplitude ratio, the error due to phase variations from the fixed offset, and the dispersion in the MW amplitude–period relation, with means of 0.079, 0.071, 0.04, and 0.035, respectively. The mean of σ_i for all Cepheids is 0.123 with a full range of 0.062–0.175; individual values are given in Table 3. Using measurement errors derived from the fit residuals instead of the photometry errors increases the mean total error by 3% with negligible impact to subsequent results.

The χ^2 is 229 for 224 degrees of freedom, a ratio of 1.02, showing that the parameter-free model is a good fit to the data. We measure 12 of 224 amplitudes to be negative but none significantly so (all $<1.5\sigma$ from 0), which may be attributed to true amplitudes $\sim$0 in the presence of photometry noise.

4.3. Constraining Departures from the Crowding-amplitude Relation

We can use the amplitude data to constrain the size of a systematic over- or underestimate of Cepheid crowding allowing for a difference, γ, between the crowding at the position of the Cepheid $\Delta m_H + \gamma$ and the value inferred nearby, Δm_H,

$$\chi^2(\gamma) = \sum_{i=1}^{n} \left(\frac{A'^H}{A'^V} - \frac{A^{H,\mathrm{MW}}}{A^{V,\mathrm{MW}}} 10^{-0.4*(\Delta m_H - \Delta m_V + \gamma)} \right)^2 \sigma_i^{-2}. \quad (15)$$

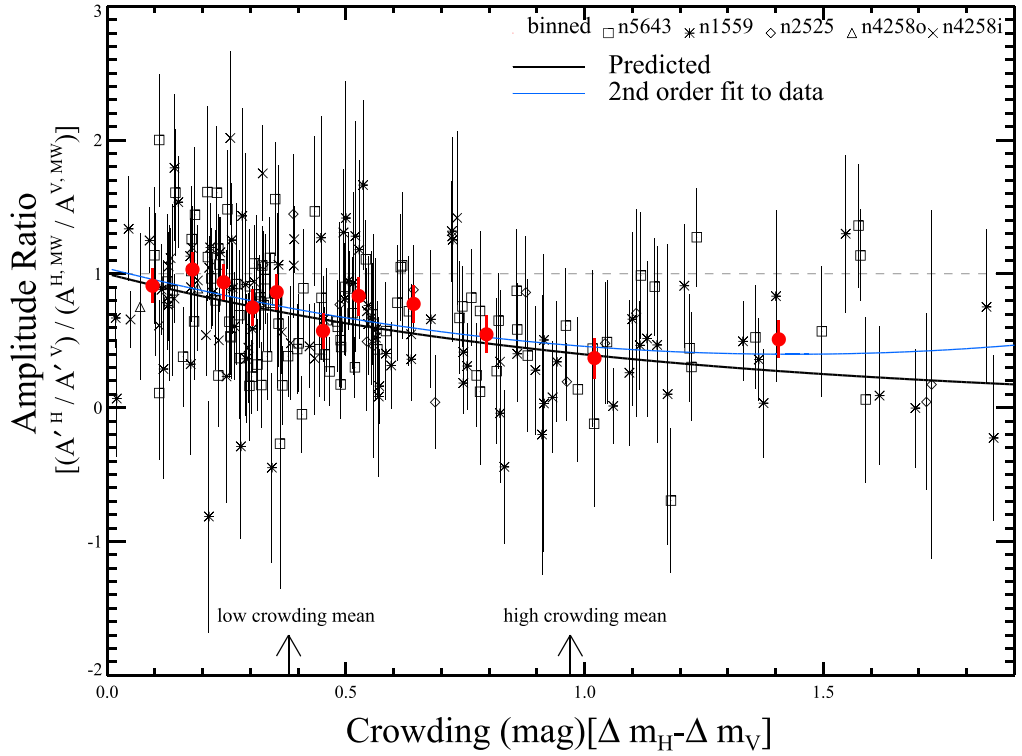

Figure 5. Amplitude ratios vs. crowding of Cepheids for four hosts. The *x*-axis is the local crowding measured as the difference between the input and recovered magnitudes for artificial stars. In practice this term is dominated by the NIR crowding term, Δm_H. The *y*-axis is the ratio of amplitudes for extragalactic Cepheids compared to MW Cepheids at the same period. The predicted trend is given by Equation (9) with no free parameters and is plotted as the black line. A quadratic fit to the data (blue line) gives similar results showing that the locally measured crowding is, on average, a good approximation to the true crowding of the Cepheid. The dashed line is plotted for guidance. The median Δm_H for the "low-crowding" sample used to measure H_0 (R16) is 0.38 mag and for the "high-crowding" sample, which is not typically used to measure H_0 but added here to increase our sensitivity to study crowding is 0.97 mag.

Table 3
Amplitude and Crowding Data for Extragalactic Cepheids

ID	Host	Log P	Δm_V	Δm_H	A^V	A^H	σ^a
137184	n5643	1.2775	−0.008	1.012	0.722	−0.030	0.154
359695	n5643	1.3822	0.006	0.548	1.073	0.451	0.119
322246	n5643	1.8627	0.031	0.215	0.396	0.257	0.091
351118	n5643	1.4188	−0.025	0.531	0.995	0.270	0.147
203310	n5643	1.3248	0.016	1.134	0.771	0.275	0.132

Note.
[a] Combined error, σ_i for Equations (14–17) including dispersion in MW relation, 0.05 intrinsic scatter, and propagated uncertainty in Δm_H.
(This table is available in its entirety in machine-readable form.)

Minimizing χ^2 yields $\gamma = 0.029 \pm 0.037$ mag as shown in Figure 7. Thus, to a precision of $\sigma \leqslant 0.04$ mag, the mean NIR crowding at the position of the Cepheid matches that inferred from nearby regions. This rules out at 5σ a systematic misestimate of Cepheid crowding as a primary cause of the well-known 0.2 mag discrepancy between local and cosmological estimates of H_0 (Riess 2019); see Section 5 for more details. Following Anderson & Riess (2018) we can also place a constraint on the fraction of Cepheids in clusters as less than 25% at >95% confidence.

The unique value of the amplitude data is as a measure of the crowding of Cepheids. However, as an alternative to this analysis we can test whether extragalactic Cepheid amplitudes match those of MW Cepheids by allowing for a rescaling of the MW Cepheids, α, to best match the extragalactic sample, accounting for crowding locally, by minimizing the following statistic:

$$\chi^2(\alpha) = \sum_{i=1}^{n}\left(\frac{A'^H}{A'^V} - \alpha\left\{\frac{A^{H,\mathrm{MW}}}{A^{V,\mathrm{MW}}}10^{-0.4*(\Delta m_H - \Delta m_V)}\right\}\right)^2 \sigma_i^{-2} \quad (16)$$

We find a best-fit value of $\alpha = 1.027 \pm 0.035$ shown in Figure 7. That is, the amplitudes ratios of MW and extragalactic Cepheids at the same periods agree to $\leqslant$4% precision.

5. Discussion

There are presently three routes for geometrically calibrating the luminosity of Cepheids empirically and in a single photometric system to better than 2% precision: with masers in NGC 4258, detached eclipsing binaries in the LMC, and

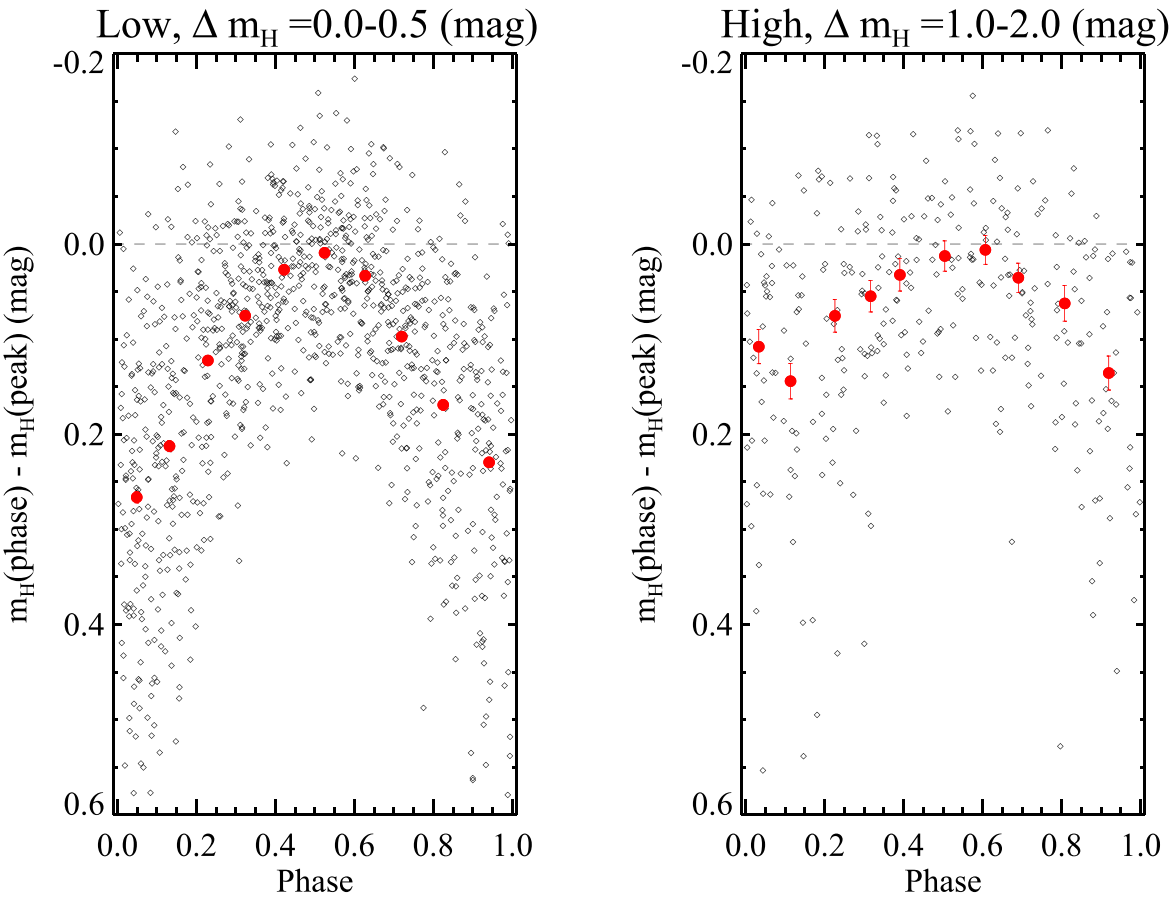

Figure 6. Composite NIR light curves in low- and high-crowding bins. Left panel: low-crowding cases, composite light curve has MW-like amplitude. These Cepheids are representative of those used for the distance scale. Right panel: high-crowding cases, composite light curve amplitude noticeably diminished. Objects with this level of crowding are typically not used for the distance scale.

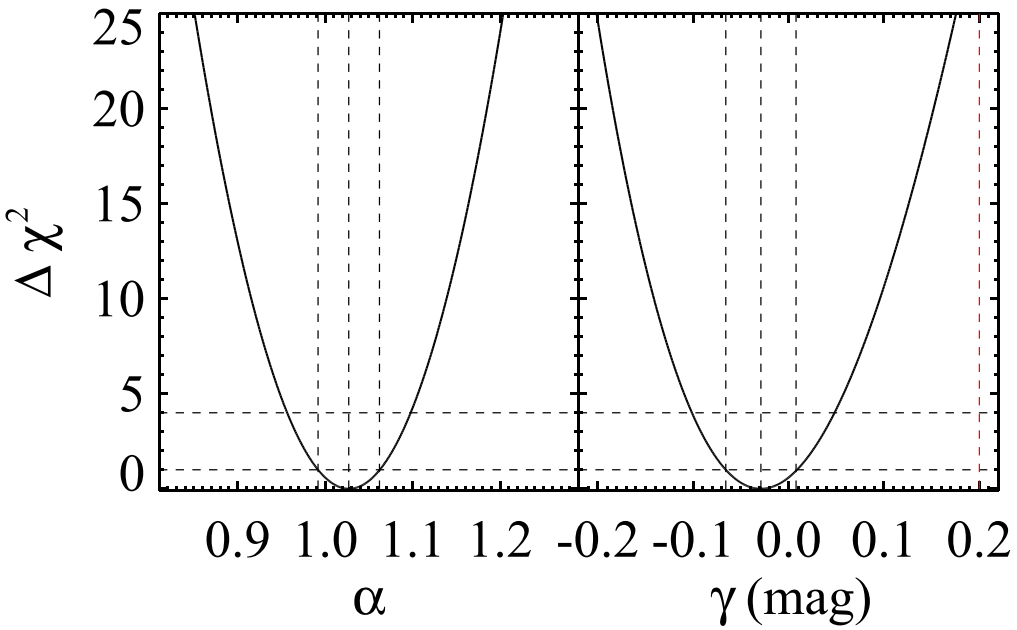

Figure 7. χ^2 tests of the amplitude and crowding data. Left: allowing for a best rescaling, α, of the MW Cepheid amplitudes to match extragalactic as in Equation (16). Right: allowing for difference between the crowding at the position of the Cepheid vs. a local determination, γ, as described in Equation (15). The vertical dashed lines shown the best fit and the $\pm 68\%$ confidence regions defined by $\Delta\chi^2 = 1$. The red vertical line shows level needed to solve the Hubble tension.

parallaxes in the MW. In the context of crowding as a source of systematic uncertainty, NGC 4258 and specifically its inner region offers the "advantage" that its Cepheids suffer similar crowding as those in SN Ia hosts. Therefore, a systematic over- or underestimate of Cepheid crowding would be expected to cancel in the measurements of Cepheids along the distance

ladder. At present all three routes offer similar precision and more than enough to verify the present Hubble tension, so the route via NGC 4258 offers valuable confirmation in the presence of crowding. The amplitude measurements presented here allow us to rule out a mis-estimate of Cepheid crowding large enough to explain the tension at $\sim 5\sigma$ confidence level. A restatement of this result in terms of what is measured is that extragalactic Cepheid amplitudes would need to be $\sim$20% smaller than empirically measured to indicate additional, unrecognized crowding as a primary source of the present discrepancy in H_0. The results presented here provide the third (after the use of NGC 4258 to calibrate Cepheids and the high-resolution study of Cepheid environments in M31) and perhaps most powerful confirmation that crowding does not compromise the accuracy of H_0 measured using extragalactic Cepheids.

Looking forward, the effort to reach a 1% measurement of the local value of H_0 must increasingly rely on parallax measurements of Cepheids from the ESA Gaia mission as they offer the only means of reaching this highly sought precision. The expected precision of Gaia parallaxes and the photometric homogeneity available from HST observations of MW Cepheids (Riess et al. 2018) can produce a Cepheid luminosity calibration with $\sim$0.4% precision, provided it is not otherwise degraded. Because MW Cepheids do not suffer crowding from our vantage point (and it is difficult to simulate their photometry seen from a perspective of $D > 10$ Mpc), we need to accurately and precisely account for crowding in the measurements of extragalactic Cepheids. Therefore, Cepheid amplitudes provide a valuable means to directly test corrections for crowding measured locally. However, we note that NIR amplitude measurements are costly in terms of observing time (where a single random phase will suffice for accurate distance measurements) and their signal-to-noise ratio is only $\sim$4. Converting the amplitude constraints to individual constraints on crowding yields $\sigma = 0.55$ mag—not as precise as can be derived using the conventional approach even if they were available for all Cepheids. As a result, while providing a measure of the crowding at the position of the Cepheid whose uncertainty dominates the scatter of the period–luminosity relation, the precision of amplitude measurements is not adequate to provide enhanced precision in the determination of these relations.

Greater resolution would be valuable as well. The James Webb Space Telescope (JWST) will offer three times the resolution of HST in the NIR and thus reduce the crowding at those wavelengths by its square or about an order of magnitude in flux, to a level comparable to that of HST in the visible. Differential tests comparing Cepheid measurements between HST and JWST at similar wavelengths should provide tests of their photometry with fidelity comparable to those based on amplitudes. Continued efforts to characterize the stellar populations around Cepheids will also be important to further reduce systematics associated with background subtraction. With all three tools together we may expect enough precision and cross-checks to keep this issue of crowding from degrading the available precision in the measurement of H_0 as measurements approach 1% precision.

Support for this work was provided by the National Aeronautics and Space Administration (NASA) through programs GO-14648, 15146 from the Space Telescope Science Institute (STScI), which is operated by AURA, Inc., under NASA contract NAS 5-26555. A.G.R., S.C., and L.M.M. gratefully acknowledge support by the Munich Institute for Astro- and Particle Physics (MIAPP) of the DFG cluster of excellence "Origin and Structure of the Universe."

This research is based primarily on observations with the NASA/ESA Hubble Space Telescope, obtained at STScI, which is operated by AURA, Inc., under NASA contract NAS 5-26555.

The HST data used in this Letter are available as part of the MAST archive[6] and can be accessed at doi:10.17909/t9-3tsk-qh26.

ORCID iDs

Wenlong Yuan https://orcid.org/0000-0001-9420-6525
Lucas M. Macri https://orcid.org/0000-0002-1775-4859

References

Anderson, R. I., & Riess, A. G. 2018, ApJ, 861, 36
Eddington, A. S. 1917, Obs, 40, 290
Ferrarese, L., Silbermann, N. A., Mould, J. R., et al. 2000, PASP, 112, 177
Freedman, W. L., Madore, B. F., Gibson, B. K., et al. 2001, ApJ, 553, 47
Freedman, W. L., Madore, B. F., Hatt, D., et al. 2019, ApJ, 882, 34
Hertzsprung, E. 1926, BAN, 3, 115
Hoffmann, S. L., Macri, L. M., Riess, A. G., et al. 2016, ApJ, 830, 10
Laney, C. D., & Stobie, R. S. 1992, A&AS, 93, 93
Leavitt, H. S., & Pickering, E. C. 1912, HarCi, 173, 1
Mateo, M., & Schechter, P. L. 1989, in Proc. 1st ESO/ST-ECF Data Analysis Workshop, ed. P. J. Grosbol, F. Murtagh, & R. H. Warmels (Garching: ESO), 69
Mochejska, B. J., Macri, L. M., Sasselov, D. D., & Stanek, K. Z. 2000, AJ, 120, 810
Monson, A. J., & Pierce, M. J. 2011, ApJS, 193, 12
Riess, A. G. 2019, NatRP, 2, 10
Riess, A. G., Casertano, S., Yuan, W., et al. 2018, ApJ, 861, 126
Riess, A. G., Casertano, S., Yuan, W., Macri, L. M., & Scolnic, D. 2019, ApJ, 876, 85
Riess, A. G., Macri, L., Casertano, S., et al. 2009, ApJ, 699, 539
Riess, A. G., Macri, L. M., Hoffmann, S. L., et al. 2016, ApJ, 826, 56
Sandage, A., Tammann, G. A., Saha, A., et al. 2006, ApJ, 653, 843
Senchyna, P., Johnson, L. C., Dalcanton, J. J., et al. 2015, ApJ, 813, 31
Soszyński, I., Gieren, W., & Pietrzyński, G. 2005, PASP, 117, 823
Stetson, P. B. 1987, PASP, 99, 191
Stetson, P. B., Davis, L. E., & Crabtree, D. R. 1990, in ASP Conf. Ser. 8, Future Development of the DAOPHOT Crowded-field Photometry Package, ed. G. H. Jacoby (San Francisco, CA: ASP), 289

[6] http://archive.stsci.edu/hst/